NPS-MR-17-001

NAVAL POSTGRADUATE SCHOOL

MONTEREY, CALIFORNIA

GENERATING ACCURATE SKIN SEA SURFACE TEMPERATURE DATA FROM OBSERVATIONS MADE USING MULTIPLE PLATFORMS DURING CASPER FIELD EXPERIMENT

by

Denny P. Alappattu, Qing Wang, Ryan Yamaguchi, Richard J. Lind,

Adam J. Christman, Kipp Shearman, Harindra Joe Fernando,

Djamal Khelif, and Ivan Savelyev

June 2017

THIS PAGE INTENTIONALLY LEFT BLANK

REPORT DOCUMENTATION PAGE

Form Approved
OMB No. 0704-0188

1. REPORT DATE *(11-13-2017)*	**2. REPORT TYPE** Technical Report	**3. DATES COVERED** ***(10/10/2015-11/06/2015)***

4. TITLE AND SUBTITLE
Generating Accurate Skin Sea Surface Temperature Data from Observations Made using Multiple Platforms during CASPER Field Experiment

5a. CONTRACT NUMBER

5b. GRANT NUMBER

5c. PROGRAM ELEMENT NUMBER

6. AUTHOR(S)
DENNY P. ALAPPATTU, QING WANG, RYAN YAMAGUCHI, RICHARD J. LIND, ADAM J. CHRISTMAN, KIPP SHEARMAN, HARINDRA JOE FERNANDO, DJAMAL KHELIF, IVAN SAVELYEV

5d. PROJECT NUMBER

5e. TASK NUMBER

5f. WORK UNIT NUMBER

7. PERFORMING ORGANIZATION NAME(S) AND ADDRESS(ES) AND ADDRESS(ES)
Meteorology Department, Naval Postgraduate School, Monterey, CA.,
Moss Landing Marine Laboratories, San Jose State University, Moss Landing, CA.,
Department of Civil & Environmental Engineering & Earth Sciences, University of Notre Dame, Notre Dame, IN.
College of Earth, Ocean, and Atmospheric Sciences, Oregon State University, Corvallis, OR.
Department of Mechanical and Aerospace Engineering, University of California - Irvine, Irvine, CA.
Remote Sensing Division, US Naval Research Laboratory, Washington, DC.

8. PERFORMING ORGANIZATION REPORT NUMBER

NPS-MR-17-001

9. SPONSORING / MONITORING AGENCY NAME(S) AND ADDRESS(ES)

OFFICE OF NAVAL RESEARCH

10. SPONSOR/MONITOR'S ACRONYM(S)

11. SPONSOR/MONITOR'S REPORT NUMBER(S)

12. DISTRIBUTION / AVAILABILITY STATEMENT
Approved for public release; distribution is unlimited

13. SUPPLEMENTARY NOTES

14. ABSTRACT

The east coast field campaign of Coupled Air-Sea Processes and Electromagnetic ducting Research (CASPER) was conducted in the fall of 2015 offshore of Duck, North Carolina. CASPER observations were conceived to better our understanding of the role of coupled air-sea processes on marine atmospheric surface layer (MASL) thermodynamics and its implications on radio frequency (RF) propagation. MASL measurements during CASPER were chiefly made from research vessels and research aircraft. Continuous and synchronized observations in the study region were made from the *R/V Hugh R. Sharp* (hereafter *Sharp*) and the *R/V Atlantic Explorer* (hereafter *Explorer*). Two research aircraft, CIRPAS Twin Otter (TO) with a controlled towed vehicle (CTV) and the SAAB 340 aircraft from the Naval Research Laboratory, were also utilized to collect measurements. A fundamental and important measurement required for air-sea interaction and RF propagation research is the sea surface temperature (SST). In this context, this report consolidates the efforts taken to ensure the accuracy of SST observation made from research vessels and aircraft.

During the experiment conventional bulk SST measurements using thermistors were taken from the *Sharp* and *Explorer* from ~1 m and ~2 m below the water line, respectively. In addition to these, an Infrared SST Autonomous Radiometer (ISAR) was deployed on the *Sharp* to measure the skin sea surface temperature (skin SST). However, skin SST data loss occurred in the ISAR observations due to frequent rain and sea-spray conditions when the instrument halts sampling to protect the optics. Bulk SST can differ from skin SST up to $O(1°C)$ due to the cool skin and/or warm layer effects caused by the absorption of insolation, heat exchange with the atmosphere, and subsurface turbulent mixing. Skin SST is the water temperature relevant in studies related to air-sea interaction and needs to be used in MASL applications instead of bulk SST. In the absence of skin SST, it is appropriate to use bulk SST adjusted for cool skin and warm layer effects. Accurate representations of skin temperature from the *Sharp* and *Explorer* bulk SST datasets are required for further CASPER interdisciplinary research.

Two different procedures were used to create corrected SST datasets from *Sharp* and *Explorer* observations. Bulk-skin SST difference and the factors governing its variability were used to correct the *Sharp* bulk SST for cool skin and warm layer effects. This corrected bulk SST is used to fill data gaps in the skin SST and create a corrected composite SST dataset for *Sharp*. The relationship between *Explorer* bulk SST and the *Sharp* corrected composite SST when the ships were within 5 km of each other was used to adjust *Explorer* bulk SST observations and make them equivalent to *Sharp* corrected composite SST.

MASL observations included 137 and 159 rawinsondes launched from the *Sharp* and *Explorer*, respectively, for boundary layer profiling. Since SST measurements are required for many applications using rawinsonde data, SST data points were appended to the rawinsonde profiles from the corrected SST datasets (T_{hs_cc} and T_{ae_bc}) generated from *Sharp* and *Explorer*.

Different instruments were used onboard the TO/CTV and SAAB 340 for SST measurements. TO/CTV sampled infrared radiation from both the ocean surface and sky so corrections could be made to compensate for the reflected portion of "sky" infrared irradiance in the measured SST data. Differences between corrected and measured SST was as large as0.5 °C under clear sky conditions.

Raw infrared signals from the SAAB 340 longwave infrared camera were converted to temperature using laboratory-based calibration curves. New offset values were determined by comparing measurements from SAAB with *Sharp* and buoy measurements as the original SSTs from SAAB were cooler by ~4 °C when compared with other collocated platforms. A corrected SST dataset from the SAAB was produced by averaging the swaths in 100 m increments.

15. SUBJECT TERMS
CASPER, Sea surface temperature, Air-sea interaction, RF propagation, Marine atmospheric surface layer.

16. SECURITY CLASSIFICATION OF:			**17. LIMITATION OF ABSTRACT**	**18. NUMBER OF PAGES**	**19a. NAME OF RESPONSIBLE PERSON**
a. REPORT	**b. ABSTRACT**	**c. THIS PAGE**			Denny P. Alappattu
Unclassified	Unclassified	Unclassified	UU	39	**19b. TELEPHONE NUMBER *(include area code)*** 831-656-3274

Standard Form 298 (Rev. 8-98)
Prescribed by ANSI Std. Z39.18

NAVAL POSTGRADUATE SCHOOL
Monterey, California 93943-5000

Ronald A. Route President	Steven Lerman Provost

The report entitled *"Generating Accurate Skin Sea Surface Temperature Data from Observations Made using Multiple Platforms during CASPER Field Experiment"* was funded by Office of Naval Research.

Further distribution of all or part of this report is authorized.

This report was prepared by:

Denny P. Alappattu[1,2], Qing Wang[1], Ryan Yamaguchi[1], Richard J. Lind[1], Adam J. Christman[3], Kipp Shearman[4], Harindra Joe Fernando[3], Djamal Khelif[5], Ivan Savelyev[6]

[1]Meteorology Department, Naval Postgraduate School, Monterey, CA.

[2]Moss Landing Marine Laboratories, San Jose State University, Moss Landing, CA.

[3]Department of Civil & Environmental Engineering & Earth Sciences, University of Notre Dame, Notre Dame, IN.

[4]College of Earth, Ocean, and Atmospheric Sciences, Oregon State University, Corvallis, OR.

[5]Department of Mechanical and Aerospace Engineering, University of California - Irvine, Irvine, CA.

[6]Remote Sensing Division, US Naval Research Laboratory, Washington, DC.

Reviewed by:	**Released by:**
Wendell A. Nuss, Chairman Meteorology Department	Jeffrey D. Paduan Dean of Research

THIS PAGE INTENTIONALLY LEFT BLANK

I. INTRODUCTION

The east coast field experiment segment of Coupled Air-Sea Processes and Electromagnetic ducting Research (CASPER) was conducted offshore of Duck, North Carolina (NC) during the Fall of 2015 (10 October to 06 November 2015). Major objectives of the experiment were to investigate the role of coupled air-sea interaction processes on boundary layer thermodynamic gradients and to study atmospheric effects on radio frequency (RF) propagation in the coastal environment. Measurements were made using multiple platforms including two research vessels, two research aircraft and a shore site at Duck, NC (Wang et al., 2017). R/V *Hugh R. Sharp* (hereafter *Sharp*) and R/V *Atlantic Explorer* (hereafter *Explorer*) were the research vessels and CIRPAS Twin Otter and NRL SAAB 340 were the research aircraft employed for the observations. Simultaneous and coordinated measurements of marine atmospheric surface layer (MASL) variables and RF propagation properties were made during the experiment. Sea surface temperature (SST) observations were also made from the research vessels and aircraft, which is a key parameter for both air-sea interaction and RF propagation studies (e. g., Alappattu et al., 2016). The accuracy of the SST datasets from these platforms is important for further studies using CASPER data.

A. SST OBSERVATIONS FROM RESEARCH VESSELS

Figure 1 shows the cruise tracks of the *Sharp* (red) and *Explorer* (blue). The location of Duck, NC is the green filled circle in the map. During CASPER, the two ships made synchronized measurements while they were within ~50 km of each. The ship tracks were along a line at ~36.18°N latitude. During a few days of observations in the Gulf Stream (GS) region (east of ~74.6°W), the vessels followed a different course (Figure 1).

SST measurements are sensitive to the observation method and two methods were used from *Sharp* to collect SST data. The first method was the conventional SST measurement using a thermistor. This sensor measures water temperatures from about one meter below the water line. Observations taken from a few centimeters to a few meters below the surface is referred to as bulk SST. The time resolution of Sharp bulk SST measurements was 10 s. The second method was with an infrared radiometer known

as Infrared SST Autonomous Radiometer (ISAR), which remote senses the water temperature at the ocean skin layer. The temperature at the atmosphere-ocean interface is the skin SST (T_s). Time resolution of the ISAR skin SST measurements was 3 minutes. Unlike the *Sharp*, only bulk SST observations using the thermistor were available from the *Explorer*, which were measured ~2 m below the water line.

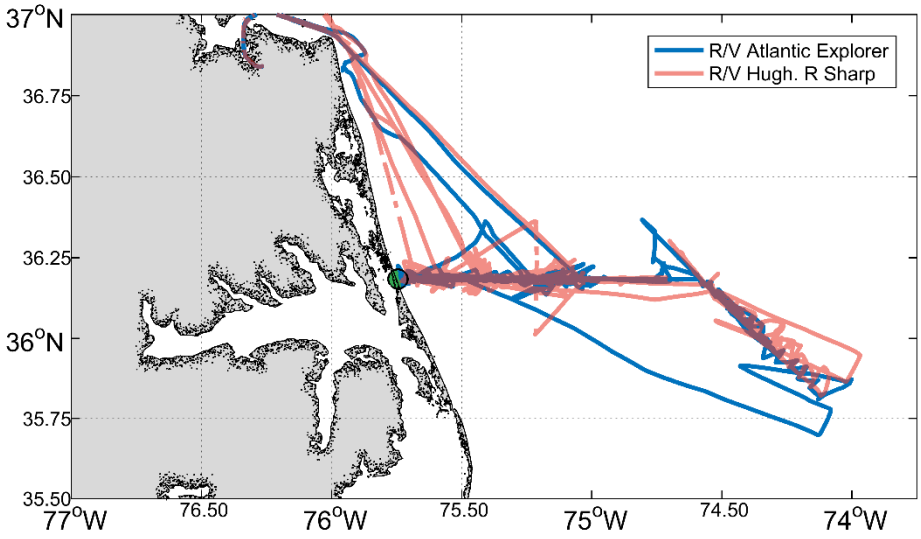

Figure 1: Region of CASPER-East field campaign overlaid with tracks traced by Explorer (blue) and Sharp (red). Location of Duck, North Carolina is shown by green filled circle.

Depending on measurement depth and prevailing conditions, bulk and skin SSTs can differ anywhere from a few tenths of a degree to $O(1°C)$ (Minnett et al., 2011; Gentemann and Minnett, 2008; Minnett, 2003; Donlon et al., 2002; Fairall et al., 1996; Schluessel et al., 1990). Differences between the skin and bulk SSTs are caused by two known processes: the warm layer and the cool skin effects (Minnett et al., 2011; Minnett et al., 2003; Donlon et al., 2002; Fairall et al., 1996). The cool skin layer of the ocean is produced by the combined cooling effects of net longwave irradiance, sensible heat flux, and latent heat flux. The surface skin layer of the ocean, much less than 1 mm thick (Minnett, 2011; Hanfin, 2002; Hanafin and Minnett, 2001; Fairall et al., 1996), is nearly always cooler than the underlying water because heat flux is generally directed from the ocean to atmosphere. The warm layer is a region in the upper few meters of the ocean where absorption of solar radiation causes considerable warming relative to the deeper mixed layer. Warm layers occur during the day when temperature stratification caused by

the absorption of solar radiation is sufficiently strong to suppress shear induced mixing from below.

Skin SST is directly related to air-sea coupling processes and is preferred in MASL applications instead of bulk SST. In the absence of skin SST measurements, it is desirable to use the bulk SST measurements adjusted for cool skin and warm layer effects (Fairall et al., 1996; Fairall et al., 2003). Previous studies have shown that failure to account for differences between bulk and skin SST can lead to significant errors in many applications, including air-sea exchange of heat fluxes and evaporation duct height (e.g. Frederickson et al., 1994).

Radiometric skin SST measurements are sensitive to rain and aerosols (mainly sea spray), leading to errors under rainy and severe sea spray conditions. Due to frequent rain and heavy sea spray conditions during CASPER, skin SST data measured from the *Sharp* by ISAR were not continuous. On the other hand, bulk SST measurements were more complete with minimal missing data compared to skin SST. One of the objectives is to have accurate and continuous SST data to represent the skin temperature from *Sharp* and *Explorer*, which are needed for RF propagation and air-sea interaction studies. Procedures followed to ensure the accuracy of SST datasets from the *Sharp* and *Explorer* are documented in this report.

Two approaches were adopted to generate the SST datasets from *Sharp* and *Explorer* observations. Since bulk and skin SST measurements were both available from the *Sharp*, bulk-skin SST differences and the factors governing their variability are used to correct the bulk SST for cool skin and warm layer effects. Corrected bulk SST is used in the absence of skin SST to create a corrected composite SST dataset for *Sharp* observations. The result is a continuous SST dataset with minimal data gaps compared the original skin SST observations. For *Explorer* measurements, the relationship between *Explorer* bulk SST and the *Sharp* corrected composite SST was examined. Data used were limited to those when the ships were within 5 km of each other. This relationship was used to adjust *Explorer* bulk SST observations to make them equivalent to *Sharp* corrected composite SSTs. Corrected *Explorer* bulk SSTs were compared with the modeled skin SSTs calculated from the bulk SSTs using the cool skin/warm layer model used in COARE bulk flux algorithm.

B. SST OBSERVATIONS FROM RESEARCH AIRCRAFT

Radiometric SST (T_{irs}) observations were taken onboard TO and CTV using downward looking Heitronics KT19 and Heitronics 15D infrared radiometers respectively. Downward-looking radiometers often underestimate the actual SST values because, in addition to the upwelling infrared radiation from the sea surface the radiometers also detect the reflected portion of downwelling (sky) infrared radiation. Radiometric SST measurements must be corrected for the effect of reflected downwelling longwave radiation. The ISAR used on *Sharp,* performs this correction automatically during data acquisition by alternately detecting the radiation from the sea surface and sky. For the TO/CTV, this correction was done through post processing of data.

The second research aircraft, SAAB 340, was operated by the Remote Sensing Division of Naval Research Laboratory. In coordination with the rest of CASPER platforms, the aircraft performed eight surveys over the primary CASPER survey line along ~36.18°N. Two of them were over the GS region. Ocean surface imagers operating in the microwave, infrared, and the visible ranges of electromagnetic spectrum were employed onboard SAAB for data collection. The SST data described in this report were obtained using longwave infrared (LWIR) camera, 'ATOM 1024' (1024x768 pixels, 30 Hz, 8-14 microns, 50 m K sensitivity) from Sofradir-EC, Inc. This camera was calibrated in the lab using a controlled temperature black body. The calibration curve was near linear in measured range, which gives confidence in camera's ability to detect SST variations within one flight. However, reflected sky radiation, cloud cover and ambient temperatures during flights generally resulted in an offset in the absolute temperature of the ocean surface (~4°C colder), varying day to day.

Methods followed for the post processing of SST data from TO/CTV and SAAB 340 are described in section V.

II. CORRECTION OF SST FROM R/V HUGH R. SHARP

A. BULK-SKIN SST DIFFERENCE

Quality control is applied to *Sharp's* bulk SST (T_b) and skin SST (T_s) data before further analysis. Only data corresponding to the wind direction within ±30° from the ship's heading were used. Data during ship maneuvers were eliminated from the dataset. A final manual screening was performed to remove outliers, resulting in 2,123 quality-controlled samples for further analysis.

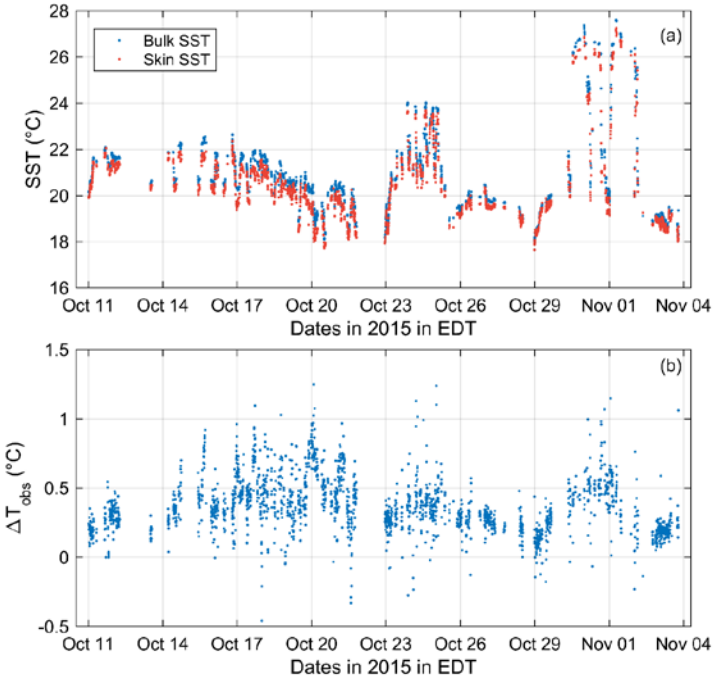

Figure 2: Time series of (a) bulk SST and radiometric skin SST and (b) bulk-skin SST difference (ΔT_{obs}) from CASPER-East measurements. Data gaps in time series are either due to the data loss in skin SST measurements or removal of data based on quality control.

Figure 2a shows bulk SST (blue) and ISAR radiometer skin SST (red) from *Sharp* measurements. Most of the time during CASPER-East, bulk SST was higher than skin SST, indicating the predominance of cool skin effects. From 29 October to 02 November, measurements were made in the western boundary of the GS and, as expected, SST in this region was highly variable with SSTs reaching 26°C on the GS side. Abrupt changes in SST in the GS region during this period resulted from measurements crossing the GS boundary.

Bulk-skin SST difference is defined as

$$\Delta T_{obs} = T_b - T_s \tag{1}$$

Observed bulk-skin SST differences (ΔT_{obs}) are shown in Figure 2b. ΔT_{obs} range from -0.5°C to 1.2°C. Approximately 73% of ΔT_{obs} are between 0.1°C and 0.5°C and roughly

23% of ΔT_{obs} are greater than 0.5°C. Negative ΔT_{obs} constitutes only 1.5% of the data. Mean bulk-skin SST difference is 0.4°C with a standard deviation of 0.2°C.

B. FACTORS AFFECTING ΔT_{obs}

Using observations from the Atlantic Ocean, Donlon and Robinson (1997) provided a detailed study on the relationship of bulk-skin SST difference with various atmospheric and oceanic parameters. They identify wind speed as the key variable that controls the characteristics of ΔT_{obs}. Observations from other oceanic regions also confirmed the strong link between wind speed and ΔT_{obs} (e.g. Minnett, 2003; Minnett et al., 2011; Donlon et al., 2002). A similar analysis using this dataset also revealed strong dependence of bulk-skin SST difference on wind speed. Diurnal effects and net longwave radiation flux are also important in determining the variability of ΔT_{obs}. In the next sections, we describe relationships of ΔT_{obs} with these parameters.

C. RELATIONSHIP WITH WIND AND TIME OF THE DAY

Variability of ΔT_{obs} with respect to wind speed and local time are shown in Figure 3. Higher (>0.5°C) ΔT_{obs} occur predominantly when the wind speed is less than ~4 m s^{-1}. ΔT_{obs} tend to be less than 0.5°C for higher wind speeds. For low wind speeds (< ~4 m s^{-1}) cases, variability of ΔT_{obs} shows a diurnal signature. When winds are below 4 m s^{-1}, ΔT_{obs} in excess of 0.5°C occur only before sunrise and after ~1500 EDT. Higher ΔT_{obs} occur only when winds are less than 1-1.5 m s^{-1}.

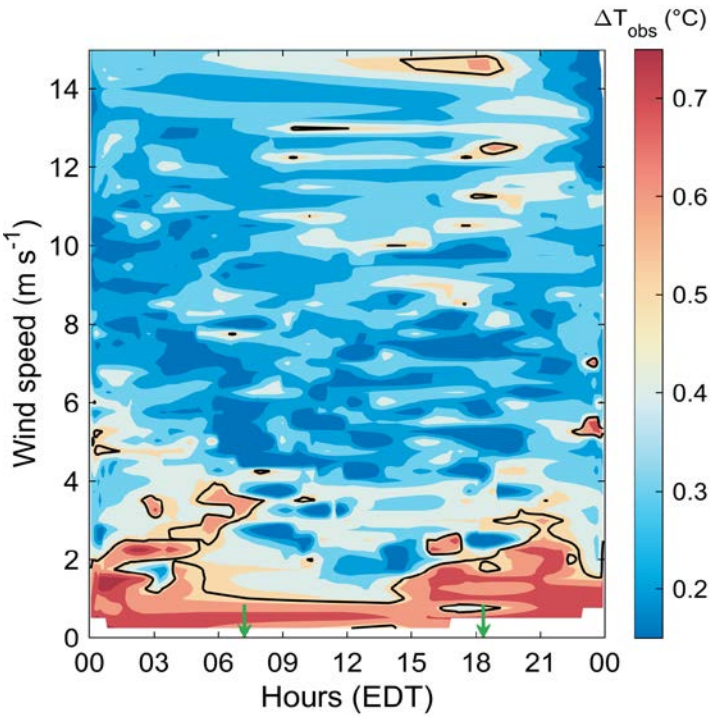

Figure 3: Variability of ΔT_{obs} with respect to local time (EDT) of observation and wind speed. The two green arrows denote sunrise and sunset times.

D. DEPENDENCE ON NET LONGWAVE RADIATION

The scatter plot of net longwave radiation versus ΔT_{obs} is shown in Figure 4 (blue dots) with a linear fit to the data shown by the red line. Bulk-skin SST difference increases with net long wave radiation flux. Occurrence of higher (>0.5°C) ΔT_{obs} increases considerably for R_{nl} values higher than ~80 W m^{-2}. Increase in net longwave radiation flux results in enhanced radiative cooling of the ocean surface leading to a further reduction in skin SST, and increasing the bulk-skin SST difference.

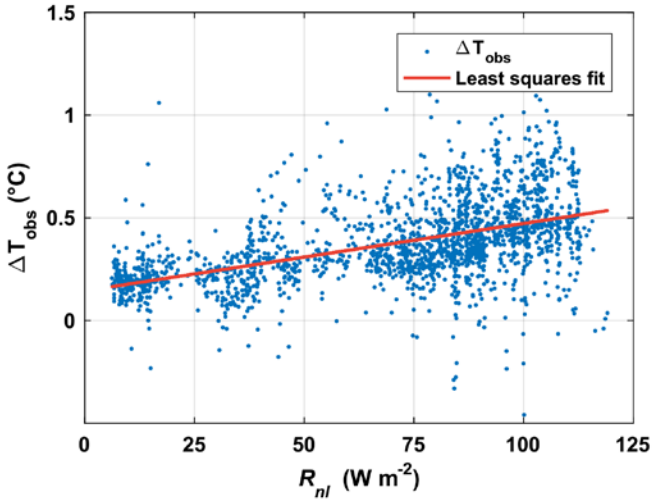

Figure 4: Scatter plot between net longwave radiation flux and ΔT_{obs}.

E. CORRECTION FOR WIND SPEED DEPENDENCE

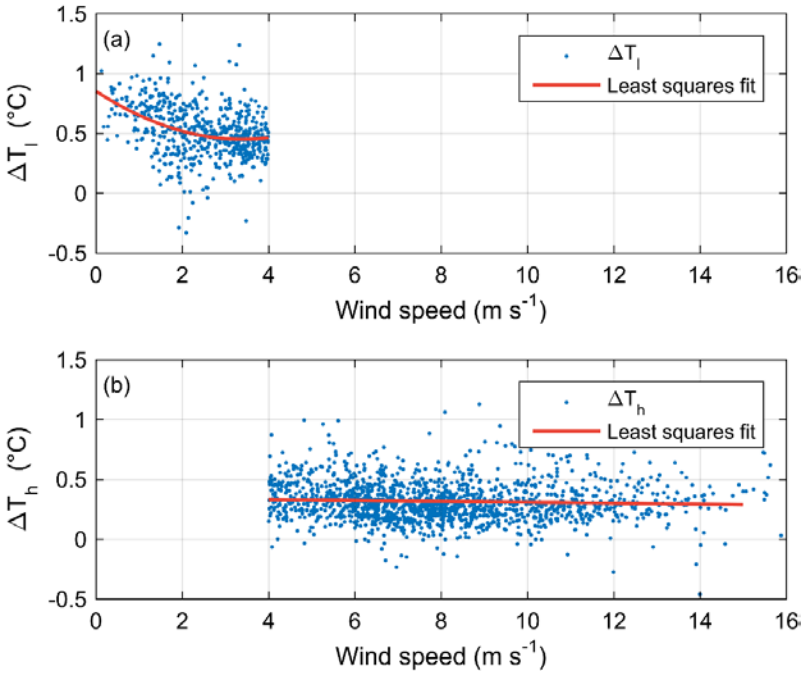

Figure 5: Wind speed dependence of (a) ΔT_l and (b) ΔT_h

Low wind speed (U) dependence of bulk-skin SST difference for low winds is described by a quadratic function (Shown in red curve Figure 5a) given by,

$$\Delta T_{l\_w} = 0.035U^2 - 0.24U + 0.85 \quad (2)$$

Above 4 m s^{-1} ΔT_h shows a nearly linear relationship with wind speed (Figure 5b). The parameterization that best fits the SST measurements under these conditions is

$$\Delta T_{h\_w} = -0.0037U + 0.35 \quad (3)$$

ΔT_l and ΔT_h variability were examined after applying the wind speed correction by subtracting the wind speed related temperature difference (ΔT_{l_w} and ΔT_{h_w}) from the corresponding bulk SST values (T_{bl} and T_{bh}). Bulk SST, after the wind based correction for low winds, can be written as

$$T_{bl\_w} = T_{bl} - \Delta T_{l\_w} \quad (4)$$

and for high winds,

$$T_{bh\_w} = T_{bh} - \Delta T_{h\_w}. \quad (5)$$

The resulting bulk-skin SST differences corresponding to low and high wind speeds after the first correction are

$$\Delta T_{l\_1} = T_{bl\_w} - T_{sl} \quad (6)$$

and

$$\Delta T_{h\_1} = T_{bh\_w} - T_{sh} \quad (7)$$

F. CORRECTION FOR DIURNAL VARIABILITY

In Figure 6, the blue dots are the ΔT_{l_1} values were calculated as described in the previous section and a sinusoidal function best fits the diurnal variability of ΔT_{l_1}. The sine function fitted to the data, shown as red curve in Figure 6, is given by

$$\Delta T_{l\_d} = 0.11 \times \sin(10.35t + 0.67) \quad (8)$$

where t is the local time (EDT) of observation.

Similar to Eqn (6), the bulk SST for low winds after the diurnal correction can be defined as

$$T_{bl\_d} = T_{bl\_w} - \Delta T_{l\_d}. \quad (9)$$

Note here that ΔT_{l_d} is subtracted from T_{bl_w}, which has been previously corrected for wind speed dependence. Finally, the temperature difference corresponding to low wind speeds after the diurnal correction is

$$\Delta T_{l\_2} = T_{bl\_d} - T_{sl} \qquad (10)$$

Since no second correction is needed to account for diurnal variations under high wind conditions, the composite of ΔT_{l_2} and ΔT_{h_1} becomes the bulk-skin SST difference after applying the corrections. We denote this composite temperature difference as ΔT_{wd}. Similarly, the composite of bulk SST corrected for wind speed and diurnal variability is denoted as T_{b_wd}, which is the composite of T_{bl_d} and T_{bh_w}.

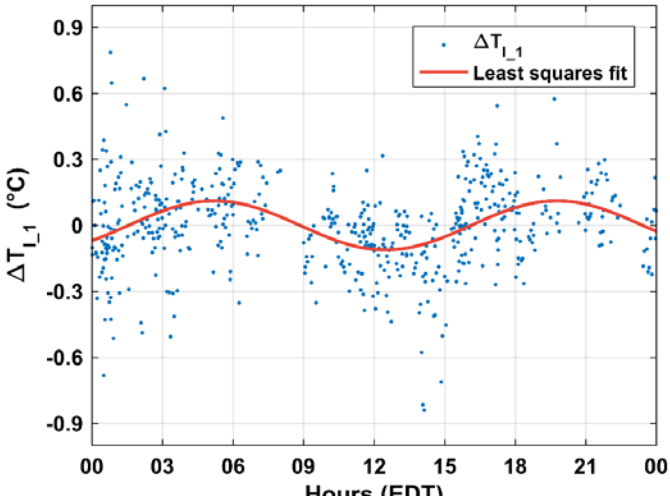

Figure 6: Variability of ΔT_{l_1} with respect to local time and sine fit.

G. CORRECTION FOR NET LONGWAVE RADIATION

The relationship between the net longwave radiation flux and the bulk-skin SST difference observed in the CASPER data suggests that ΔT_{wd} (bulk-skin SST difference

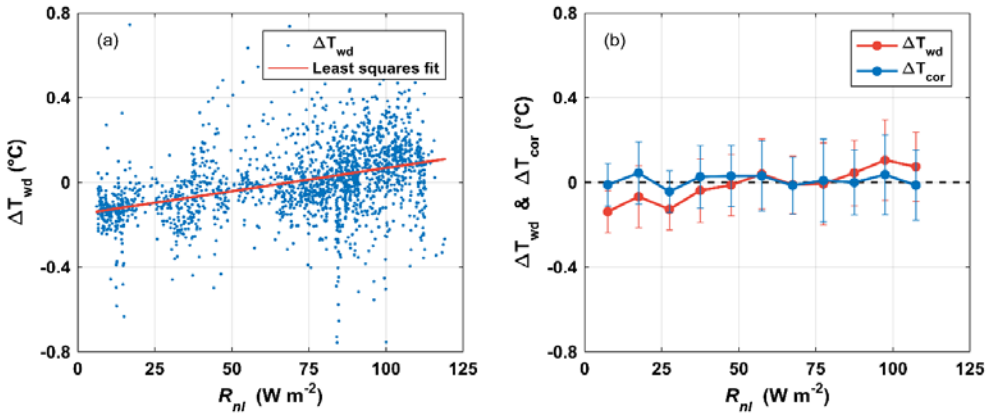

Figure 7: (a) Scatter plot between net longwave radiation flux and ΔT_{wd} and (b) variability of bin averaged ΔT_{wd} and ΔT_{wd} with respect to net longwave radiation flux.

after applying the wind and diurnal corrections) also shows an increasing trend with net longwave radiation flux (Figure 7a), even though the above procedures considerably

reduced the bias. A linear fit (red line in Figure 7a) having the following form (Eqn 11) was found to represent the dependence of ΔT_{wd} variability on R_{nl}.

$$\Delta T_r = 0.002 R_{nl} - 0.15 \quad (11)$$

Bulk SST after quantifying the ΔT_{wd} for its dependence on R_{nl} is given by,

$$T_{b\_cor} = T_{b\_wd} - \Delta T_r \quad (12)$$

Corresponding bulk-skin SST differences can be written as,

$$\Delta T_{cor} = T_{b\_cor} - T_s \quad (13)$$

In Figure 7b, bin averages of the temperature difference after quantifying for the dependence on net longwave radiation (ΔT_{cor}) is shown in blue. The red curve is the bin average of ΔT_{wd}. Error bars are the one standard deviation of the data in each bin. It can be seen that, in comparison to the ΔT_{wd} (red curve), ΔT_{cor} (blue curve) lies close to the zero line, and ΔT_{cor} variability is independent of net longwave radiation flux. Before correction, the mean of ΔT_{obs} was 0.4°C and following correction, the mean of ΔT_{cor} reduced almost to 0°C. This empirical method effectively adjusts *Sharp's* bulk SST data to the skin SST.

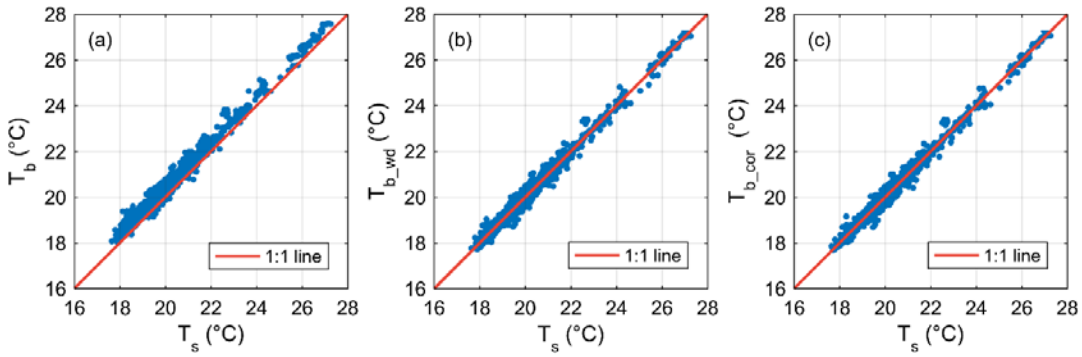

Figure 8: Scatter plot between skin SST and bulk SST (a) before correction (b) after correction for wind speed dependence and diurnal variability and (c) after final correction for dependence on net longwave radiation flux.

Figure 8a is the scatter plot between radiometric skin SST (T_s) and observed bulk SST (T_b). Data points consistently lie to the T_b side of the red line representing a positive bias in bulk SST compared to the observed radiometric skin SST. Figures 8b and 8c show the scatter plot between T_{b_wd} versus T_s and T_{b_cor} versus T_s respectively. In comparison to Figure 8a, data points lie along the 1:1 line in Figures 8b-c. This suggests that our method is effective in removing the cool skin and warm layer effects from the bulk SST

data. It should be noted that there is no significant difference between Figures 8b and 8c. This is because the wind speed and diurnal corrections are able to reduce the bulk-skin SST difference significantly. Therefore, in the absence of longwave radiation data, which is often the case with bulk SST measurements, the wind speed and diurnal corrections applied to the bulk SST can provide a good approximation for skin SST.

H. CORRECTED BULK SST AND COMPOSITE

The method above was applied to all the available *Sharp* bulk SST data. In Figure 9a, the red and green dots represent observed bulk SST and corrected bulk SST. Mean *Sharp* bulk SST is reduced by 0.3°C (from 21.1°C to 20.8°C) by the correction. A composite corrected bulk SST dataset was produced by replacing missing/erroneous skin SST with data from ISAR, and this is denoted as *Sharp* corrected composite SST (T_{hs_cc}). This dataset has a time resolution of five minutes. The time series of T_{hs_cc} is shown in Figure 9b.

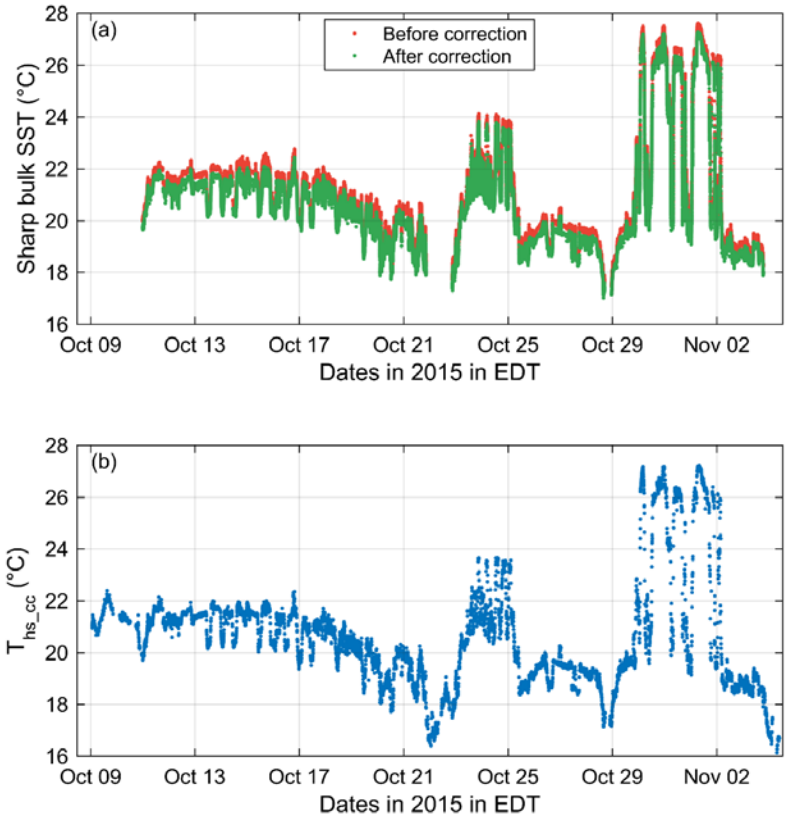

Figure 9: Time series of (a) all the available Sharp bulk SST before and after correction and (b) the Sharp corrected composite SST

THIS PAGE INTENTIONALLY LEFT BLANK

III. CORRECTION OF SST FROM R/V ATLANTIC EXPLORER

Radiometer skin SST measurements were not available on *Explorer*, so another approach was used to correct the *Explorer* bulk SST by comparing it with the T_{hs_cc} (shown in Figure 9b). Figure 10 shows the time series of *Explorer* bulk SST (T_{ae_b}) using blue dots. T_{hs_cc}, shown in Figure 9b is plotted again in this figure (red dots) for comparison. Remember that the two vessels were making coordinated measurements and often within close proximity during CASPER. In general, T_{ae_b} follows the variability of T_{hs_cc}. Nonetheless, the former was marginally higher than the latter most of the time. This is expected since T_{hs_cc} is composed of skin SST and the bulk SST corrected for cool skin and warm layer effects.

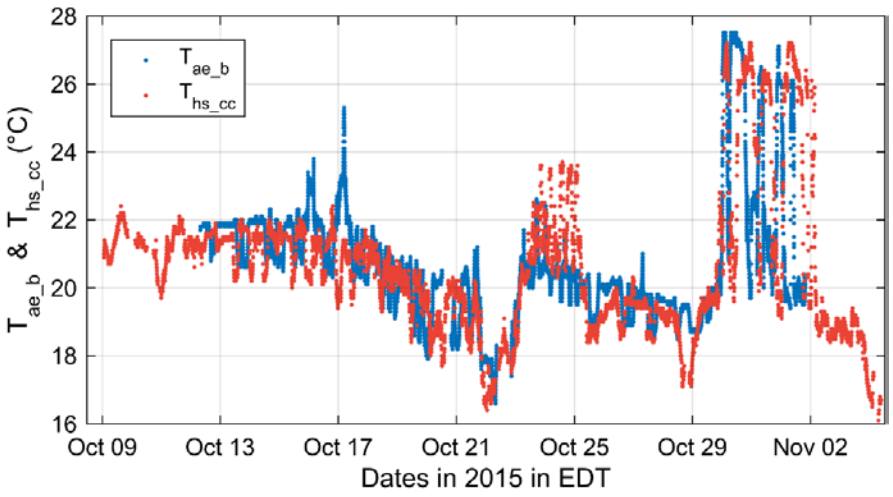

Figure 10: Time series of (a) all the available Sharp bulk SST before and after correction and (b) the Sharp corrected composite SST

A. SELECTION OF DATA POINTS FOR COMPARISON

The first step in the correction of the *Explorer* bulk SST was to select the contemporaneous SST data points from *Explorer* and *Sharp*, when the vessels were within 5 km of each other. It is reasonable to assume that the water temperature will not vary significantly within this spatial scale. This screening left behind 664 samples for further analysis. Time series of these selected data points is shown Figure 11. Blue crosses are the selected T_{ae_b} and red circles represents the corresponding T_{hs_cc}. Mean difference between the selected T_{ae_b} and T_{hs_cc} was ~0.3°C

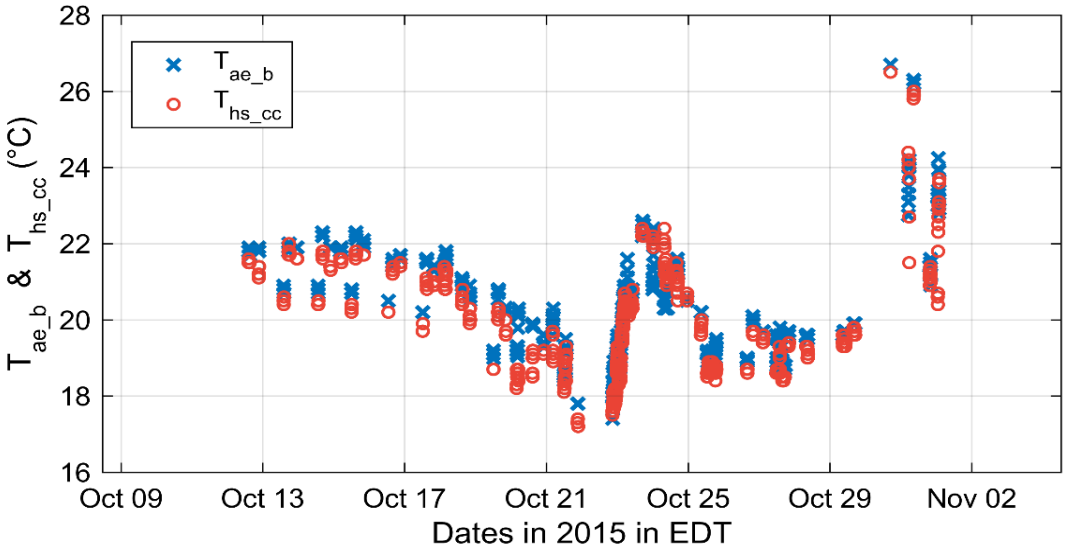

Figure 11: Time series of contemporaneous Explorer bulk SST and Sharp corrected composite SST when the ships were within 5 km radius from each other.

B. CORRECTION OF T_{ae_b} USING THE RELATIONSHIP WITH T_{hs_cc}

Figure 12a is the scatter plot between the selected T_{hs_cc} and T_{ae_b} data points with the 1:1 line is shown in red. A positive bias in T_{ae_b}, relative to T_{hs_cc} is can be seen.

A least squares linear fit represents the relationship of T_{ae_b} and T_{hs_cc}. This linear

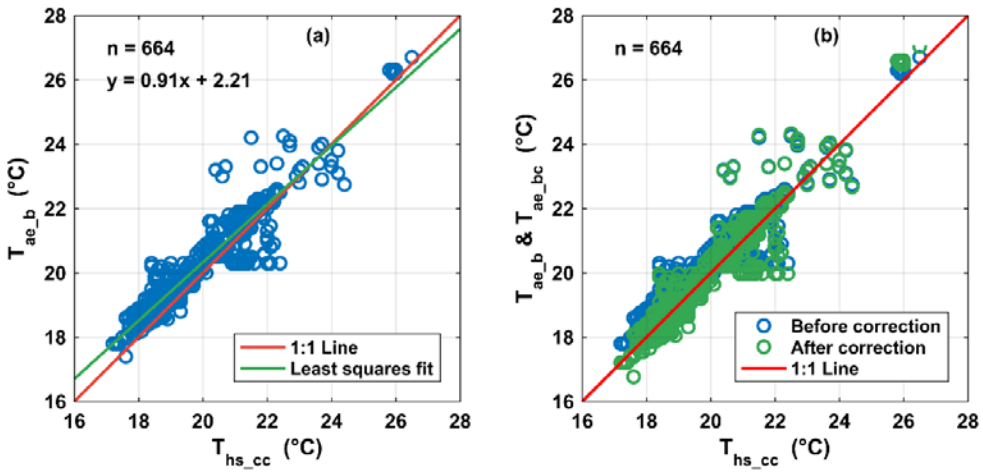

Figure 12: Scatter plot of selected sharp corrected composite SST with (a) Explorer bulk SST and sharp corrected composite SST and (b) same as (a) but including corrected Explorer SST.

regression, shown in green (Figure 12a) is,

$$y = 0.91\,x + 2.21 \tag{14}$$

Eqn (14) was applied to T_{ae_b} to make it equivalent to T_{hs_cc} as follows,

$$T_{ae\_bc} = \frac{T_{ae\_b} - 2.21}{0.91} \quad (15)$$

where T_{ae_bc} is the *Explorer* corrected bulk SST.

Scatter plots of T_{hs_cc} and *Explorer* bulk SST before (T_{ae_b}) and after (T_{ae_bc}) correction are shown in Figure 12b. The blue circles are the same as those in Figure 12a and the green circles represent the *Explorer* bulk SST after correction. After correction, T_{ae_bc} (green circles) lie symmetrically along the 1:1 line indicating the method is effective at removing the bias in the *Explorer* bulk SST when compared to the *Sharp* corrected composite SST.

Note that this correction was applied only to the selected contemporaneous SST data points when the ships were within 5 km of each other. Results of the application of Eqn (15) to all the available T_{ae_b} is shown in Figure 13, where green dots correspond to the entire *Explorer* bulk SST data after the correction (T_{ae_bc}). Observed *Explorer* bulk SST (T_{ae_b}) is shown red dots. After correction, the average difference between *Explorer* bulk SST and *Explorer* corrected bulk SST was 0.3°C.

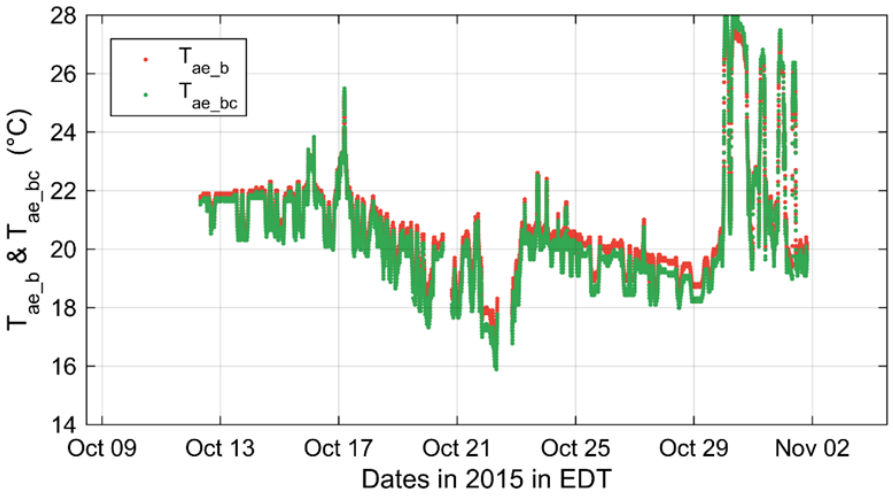

Figure 13: Time series of Explorer bulk SST before and after correction.

C. COMPARISON WITH MODELED SKIN SST

T_{ae_bc} obtained through the above correction method was compared to the modeled *Explorer* skin SST (T_{ae_sm}) generated from the T_{ae_b} using the cool skin/warm layer model used in the COARE v3.5 bulk flux algorithm. For this particular data set, given that the water intake on the *Explorer* was approximately 2 m below the water surface, it was assumed that the measured samples were taken from within the warm layer of the upper ocean. Hence, the COARE model algorithms were used only to compensate for the cool skin temperature depression. A scatter plot between T_{ae_b} and T_{ae_sm} is shown in Figure 14, with a linear fit to the data and the 1:1 line shown in green and red lines, respectively. For water temperatures less than ~22°C, T_{ae_sm} agrees well with T_{ae_bc} . Above ~ 22°C, the modeled temperature is lower than the corresponding T_{ae_bc} estimates.

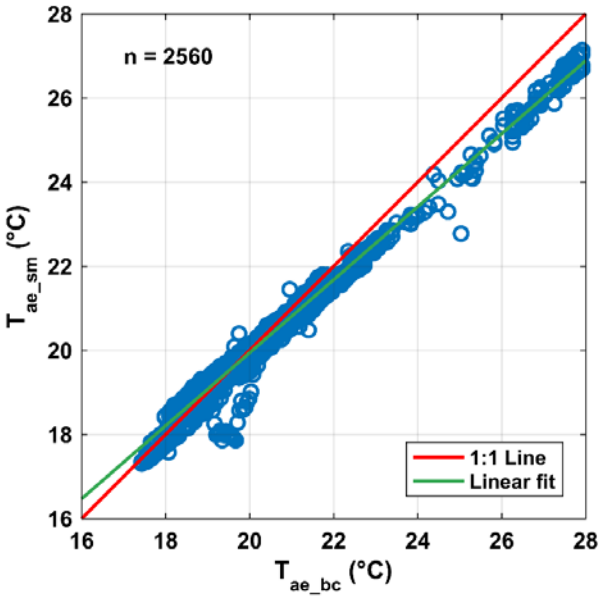

Figure 14: Scatter plot between *Explorer* corrected bulk SST and *Explorer* modeled skin SST.

IV. APPENDING SST TO RAWINSONDE MEASUREMENTS

In addition to MASL observations, boundary layer soundings using InterMet® rawinsondes were performed with 137 and 159 launches from *Sharp* and *Explorer* respectively, during CASPER. Pressure, temperature, relative humidity, and wind were recorded at one-second intervals with vertical resolution of ~5 meters. For many applications used in RF propagation studies, it is required to have the SST measurement along with the boundary layer profiles, so SST data were appended to the rawinsonde profiles from the corrected SST datasets (T_{hs_cc} and T_{ae_bc}) generated from *Sharp* and *Explorer* observations.

To fetch the SST data corresponding to each sounding, the period between time of rawinsonde launch and when the sonde reached 100 m altitude was used. SST data in this period were selected from T_{hs_cc} and T_{ae_bc} datasets depending on where the sonde was launched. Time average of this SST was assigned to the corresponding sounding. Figures 15a and 15b summarize the results of the procedure, where blue circles represent SST extracted from T_{hs_cc} (Figure 15a) and T_{ae_bc} (Figure 15b). If SST data are available for a rawinsonde launch, it is indicated by a green cross at the upper X-axis of the figures. Similarly, the red crosses in the figure indicate soundings without SST data. All soundings from the *Sharp* have corresponding SST data (Figure 15a). SST data were unavailable for 48 soundings from the *Explorer*.

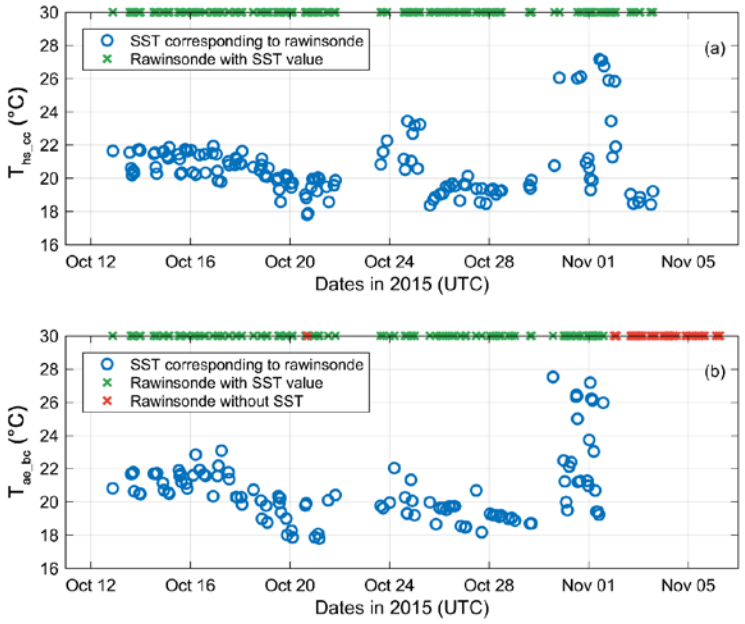

Figure 15: SST data appended to the soundings taken from (a) *Sharp* and (b) *Explorer*.

THIS PAGE INTENTIONALLY LEFT BLANK

V. CORRECTION OF SST FROM RESEARCH AIRCRAFT

A. CORRECTION OF SST FROM TWIN OTTER/CTV

The procedures outlined in Hignett (1998), Katsaros (1980) and Burns et al. (2000) were followed for the correction of radiometer SST from TO/CTV. This correction method uses infrared "sky temperature" measured by an identical upward-looking infrared radiometer. Reflected "sky" infrared irradiance was estimated from this measurement and used to compensate for its effect on the measured radiometer SST data (T_{irs}) to derive the corrected SST (T_{irsc}).

An evaluation of the correction scheme was made using data from flights conducted in two regimes: nearly clear skies and completely overcast sky conditions. The latter observations were made within the stratocumulus-topped boundary layer. Differences $T_{irsc} - T_{irs}$ were always positive (~0.47 °C) under clear sky conditions and much smaller (~0.05°C) under overcast, unbroken stratocumulus decks.

Corrected SST and difference ($T_{irsc} - T_{irs}$) time series for both TO (green) and CTV (blue) for the November 1, 2015 flight over the GS are shown in Figure 16a and 16b. The CTV was not equipped with an upward-looking radiometer, so downwelling infrared radiation data were used from TO, shifted by 10.5 s (to account for the fact that CTV flies ~580 m behind TO), to correct the SST measured by the CTV's Heitronics 15D radiometer.

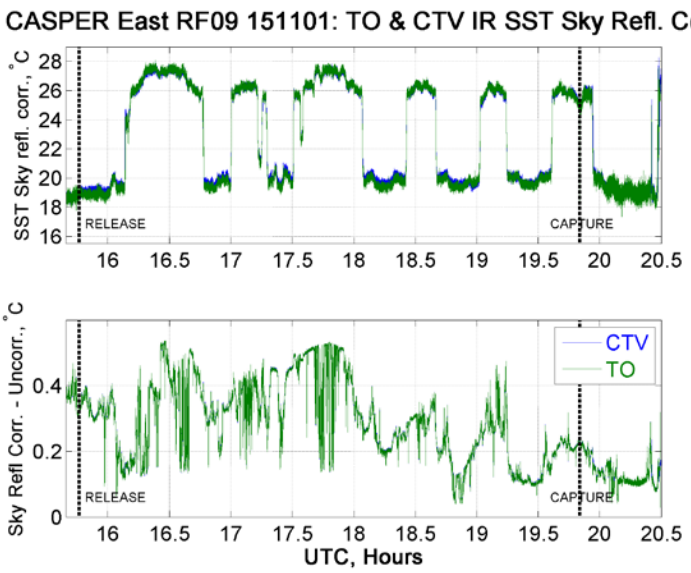

Figure 16: Radiometric SST from CTV (blue) and TO (green) after correction for reflected sky irradiance (top) and the actual correction for reflected sky irradiance (bottom).

B. SAAB SST MEASUREMENTS AND CALIBRATION

The raw infrared imagery collected by a LWIR camera onboard SAAB was accompanied by precise global positioning system data and inertial measurement unit metadata recorded by a C-MIGITS® system. This allows fully resolved flight and look angle geometry and tags each pixel with latitude and longitude over the ocean surface with ~1-2 m accuracy. The initial data product was a detailed thermal map (i.e., swath) collected along the flight track, typically tens of kilometers long and ~500-1000 m wide, depending on the aircraft's altitude. Imagery is projected onto a 1x1 m universal transverse Mercator grid for ease of processing.

As mentioned earlier, raw infrared data obtained by the camera are converted to temperature using calibration curves obtained in laboratory conditions. However, a number of additional factors exist in the field, which are expected to influence the SST estimate. These factors include, but are not limited to 1) varying ambient temperature, which affects temperature of the exposed lens; 2) atmospheric humidity and aerosols, which attenuate SST signal; and 3) background sky radiance reflected from the ocean surface, for example presence of intermittent clouds or sun glint can make accurate SST retrieval impossible.

After initial quality control, filtering, and application of temperature calibration the sum of factors listed above was found to make retrieved SST appear cooler (by ~4 °C) when compared to other collocated platforms. It was assumed that the lab calibration gain is still applicable, and that the offset was incorrect, but remained constant during each SAAB flight. A new value of offset calibration was determined by comparing collocated SST retrieved by SAAB with other more reliable measurements of SST. To determine the offset in SAAB's SST measurement, we used the *Sharp* corrected composite SST (T_{hs_cc}) dataset (see section II.H). For the seven out of eight flights conducted offshore from Duck, and on both Gulf Stream flights, we used T_{hs_cc} dataset for the comparison. The only exception is the last flight on November 04. On this date, in the absence of *Sharp* measurements we used SST measurements from the Scripps Institution of Oceanography Miniature Wave Buoy moored at 36.18°N, 75.58°W during the CASPER experiment. This process of forcing the SST retrieval to match available ground truth measurements changed the offset for each swath.

SAAB SST swaths were averaged over 100 m increments and shown in Figure 17, color coded for the eight flight days shown as a function of distance from the shore. This figure elucidates the intricate nature of SST variability in the study region. Surface temperature tends to be cooler within the first ~10-20 km (possibly due to the Chesapeake Bay plume). SSTs steady increase with distance from the shore albeit the spatial SST gradient varies with the flight date. Further from shore (beyond ~100 km) the influence of a warm water filament from GS is also noticed in the surface temperature. The occasional cold spikes are caused by ship wakes, which disrupt thermal stratification by bringing colder water to the surface.

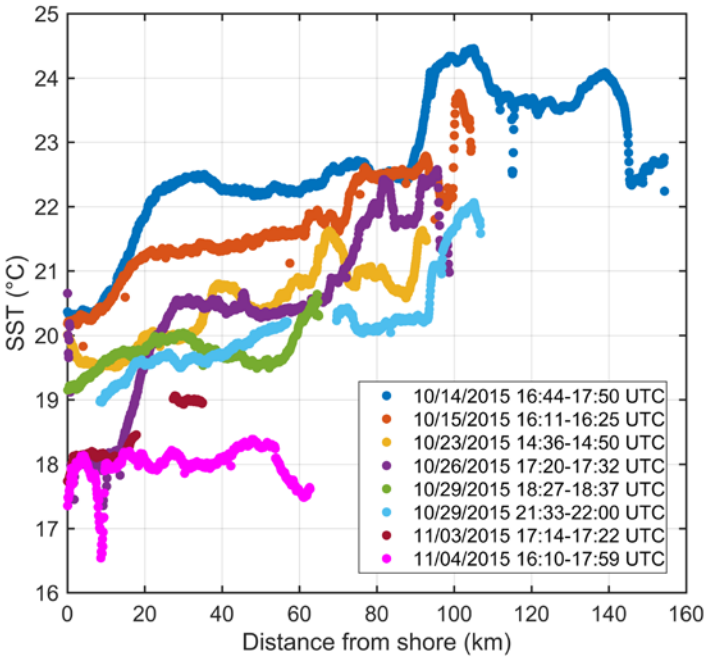

Figure 17: Sea surface temperature swaths obtained by NRL SAAB 340.

THIS PAGE INTENTIONALLY LEFT BLANK

VI. COMPARISON OF SST DATA FROM *SHARP* AND CTV

During CASPER, (1024x768 pixels, 30 Hz, 8-14 microns, 50 mK sensitivity) TO/CTV flights were conducted to coincide with the ship observations. Figure 18 depicts one the flight legs from the GS region where tracks of the TO/CTV and the *Sharp* are shown with color representing SSTs. Corrected SSTs from CTV are used here for comparison with the *Sharp* corrected composite SST. The TO/CTV track is the diagonal from the bottom right corner to the upper left corner of the figure. This flight was conducted on November 01 2015. Short lines perpendicular to the TO/CTV tracks labelled with the observation time (in UTC) are the *Sharp's* tracks. Qualitatively, corrected SST data from the CTV and *Sharp* shows good match.

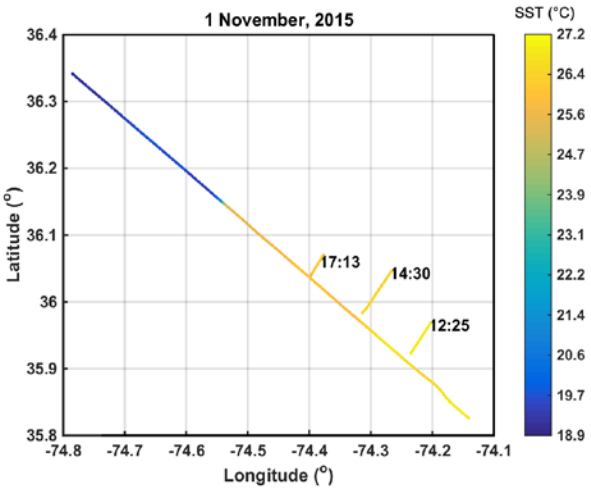

Figure 18: Comparison of CTV corrected SST with *Sharp* corrected composite SST

THIS PAGE INTENTIONALLY LEFT BLANK

VII. SUMMARY

Accuracy of SST observations is essential for many atmospheric and oceanographic applications. The skin SST is the relevant parameter that must be used in these calculations. During the CASPER field experiment, skin SST measurements were made from *Sharp* using ISAR. However, the ISAR halts measurements under rain and/or sea-spray conditions that resulted in some data loss during CASPER. Bulk SST measurements were available continuously from *Sharp* from ~1 m below the water line. Unlike *Sharp*, only bulk SST observations (from ~2 m below the water line) were available from the *Explorer*. Deriving accurate representations of skin temperature from bulk SST data became necessary for further analysis of CASPER data.

One approach of doing this is by accounting for the difference between bulk SST and skin SST. This difference often varies from a few tenths of a degree to *O*(1°C). Bulk-skin SST difference is caused by two processes known as the warm layer and cool skin effects resulting from the absorption of insolation, heat exchange with the atmosphere, and subsurface turbulent mixing. Since skin SST and bulk SST measurements were available, this method was deemed appropriate for *Sharp* measurements.

Analysis showed the variability of bulk-skin SST differences have a strong dependence on wind speed, and at wind speeds lower than 4 m s^{-1}, bulk-skin SST difference also varies diurnally. Bulk-skin SST difference also showed increasing trends with net longwave radiation flux. To correct the *Sharp* bulk SST for cool skin and warm layer effects, a three-step correction method was employed. Initially, the bulk-skin SST difference data are separated into low wind (< 4 m s^{-1}) and high wind (> 4 m s^{-1}) cases. Wind speed dependence on bulk-skin SST difference for low wind and high wind cases were then quantified separately using quadratic and linear least squares fits, respectively. A sine fit is used to quantify the diurnal signal in the bulk-skin SST difference for low wind speed cases after correction for wind speed dependence. A linear fit was used to quantify the increase in bulk-skin SST difference with net longwave radiation flux. This method reduced the mean bulk-skin SST difference to nearly zero degrees Celsius from its original value of 0.4°C. This method was applied to the all *Sharp* bulk SSTs to make

them equivalent to skin SSTs. Mean *Sharp* bulk SST was reduced by 0.3°C from 21.1°C to 20.8°C by the correction. Finally, a composite SST dataset was created by supplementing missing/erroneous skin SST data from ISAR with corrected bulk SST data from the *Sharp* measurements.

The relationship between *Explorer* bulk SST and *Sharp* corrected composite SST was used to adjust the *Explorer* bulk SST. For this, only cotemporaneous data points when the ships were within 5 km of each other were used. This relationship was applied to the entire *Explorer* bulk SST set to make it equivalent to *Sharp* corrected composite SST. Corrected *Explorer* bulk SST was compared with modeled skin SST calculated from the bulk SST using the cool skin/warm layer model used in COARE bulk flux algorithm.

In addition to the MASL observations, 137 and 159 rawinsondes were launched from *Sharp* and *Explorer*, respectively, for boundary layer sounding. Since SST measurements are required for many applications using rawinsonde data, SST data were appended to the rawinsonde profiles from the corrected SST datasets (T_{hs_cc} and T_{ae_bc}) generated from *Sharp* and *Explorer* observations.

Observations of the infrared "sky temperature" measured by the upward-looking infrared radiometer were used to compensate for the reflected portion of "sky" infrared irradiance in the measured SST data to derive the corrected SST from TO/CTV observations. Differences between corrected and measured SST were significant (~0.47 °C) under clear sky conditions.

For the SAAB, raw infrared signals from the camera were converted to temperature using calibration curves obtained in laboratory conditions, however new of offset values, determined by comparisons with collocated SSTs from *Sharp* and a buoy, were applied. This offset compensated for factors in the environment that influenced the SAAB's SST retrievals. After correction, SAAB SSTs matched well with the SST measurements from other platforms.

LIST OF REFERENCES

Alappattu, D. P., Q. Wang, and J. Kalogiros (2016), Anomalous propagation conditions over eastern Pacific Ocean derived from MAGIC data, *Radio Science*, *51*, 1142–1156, doi:10.1002/2016RS005994.

Burns, S.P., D. Khelif, C.A. Friehe, P. Hignett, A.G. Williams, A.L.M. Grant, J.M. Hacker, D.E.Hagan, Y.L. Serra, D.P. Rogers, E.F. Bradley, R.A. Weller, C.W. Fairall, S.P. Anderson, C.A. Paulson, and P.A. Coppin, 1999: Comparisons of aircraft, ship, and buoy radiation and SST measurements from TOGA COARE. *Journal of Geophysical Research*, *105*, 15,627-15,652.

Donlon, C.J., I. S. Robinson, (1997), Observations of the oceanic thermal skin in the Atlantic Ocean. *Journal of Geophysical Research*, *102*, 18585–18606.

Donlon, C.J., Minnett, P.J., Gentemann, C., Nightingale, T.J., Barton, I.J., Ward, B., Murray, J., (2002), Toward improved validation of satellite sea surface skin temperature measurements for climate research. *Journal of Climate*, *15*, 353–369

Fairall, C., Bradley, E., Godfrey, J., Wick, G., Edson, J., Young, G., (1996), Cool-skin and warm-layer effects on sea surface temperature. *Journal of Geophysical Research*, *101 (C1)*, 1295–1308.

Fairall, C., E. Bradley, J. Hare, A. Grachev, and J. Edson, (2003), Bulk parameterization of air–sea fluxes: updates and verification for the COARE algorithm. *J. Climate*, *16*, 571–591, doi: 10.1175/1520-0442(2003)016<0571:BPOASF>2.0.CO;2.

Frederickson P. A, (1994), The effect of infrared sea surface temperature measurements on evaporation duct height estimation, *Naval Postgraduate School Technical Report*, http://hdl.handle.net/10945/28715.

Gentemann, C.L., Minnett, P.J., (2008), Radiometric measurements of ocean surface thermal variability. *Journal of Geophysical Research, 113*, C08017, doi:10.1029/2007JC004540.

Hanafin, J.A., (2002), On sea surface properties and characteristics in the infrared. *Ph.D. Thesis*, University of Miami, Miami.

Hanafin, J.A., Minnett, P.J., (2001), Profiling temperature in the sea surface skin layer using FTIR measurements, In: Donelan, M.A., Drennan, W.M., Saltzmann, E.S., Wanninkhof, R. (Eds.), *Gas Transfer at Water Surfaces. American Geophysical Union Monograph*, pp. 161–166.

Hignett, P., Correction of airborne sea surface temperature measurements for non-blackness effectsMRF Tech. Note 28, 15Meteorol. Res. Flight, Hampshire, England, 1998.

Katsaros, K., Radiative sensing of sea surface temperature, Air-Sea Interaction: Instruments and Methods. Dobson, L. Hasse, R. Davis, 293–317, Plenum, New York, 1980.

Minnett, P.J., (2003), Radiometric measurements of the sea–surface skin temperature—the competing roles of the diurnal thermocline and the cool skin, *International Journal of Remote Sensing, 24*, 5033–5047.

Minnett. P J., Murray Smith, Brian Ward, (2011), Measurements of the oceanic thermal skin effect, *Deep Sea Research Part II: Topical Studies in Oceanography, 58*, 861-868, doi: 10.1016/j.dsr2.2010.10.024.

Schluessel, P., Emery, W.J., Grassl, H., Mammen, T., (1990), On the bulk–skin temperature difference and its impact on satellite remote sensing of sea surface temperatures. *Journal of Geophysical Research, 95*, 13341–313356.

Wang, Q., and Co-authors, (2017), CASPER- a multidisciplinary program on the coupled air-sea processes and electromagnetic wave (EM) ducting research, *Manuscript submitted to Bull. Amer. Meteo. Soc*.

INITIAL DISTRIBUTION LIST

1. Defense Technical Information Center
   Ft. Belvoir, Virginia

2. Dudley Knox Library
   Naval Postgraduate School
   Monterey, California

3. Research Sponsored Programs Office, Code 41
   Naval Postgraduate School
   Monterey, CA 93943